Hindawi
Geofluids
Volume 2022, Article ID 1712740, 15 pages
https://doi.org/10.1155/2022/1712740

Research Article

Study of the Influence of Clay Minerals on the Mechanical and Percolation Properties of Weakly Cemented Rocks

Shiru Guo,[1] **Hai Pu**,[1,2] **Mengsen Yang**,[1] **Ding Liu**,[1] **Ziheng Sha**,[1] **and Junce Xu**[1]

[1]*State Key Laboratory for Geomechanics and Deep Underground Engineering, China University of Mining and Technology, Xuzhou, Jiangsu 221116, China*
[2]*College of Mining Engineering and Geology, Xinjiang Institute of Engineering, Urumqi, Xinjiang 830023, China*

Correspondence should be addressed to Hai Pu; haipu@cumt.edu.cn

Received 13 April 2022; Accepted 7 June 2022; Published 20 June 2022

Academic Editor: Guang-Liang Feng

The weakly cemented rock layer is easily damaged under the combined effect of seepage and mining disturbance and creates massive engineering disasters. This paper uses the self-designed weakly cemented remodeling mechanism to prepare weakly cemented rock samples with clay minerals accounting for 20%, 30%, 40%, 50%, and 60% of the total. The MTS816 system, in conjunction with an acoustic emission system and a high-speed camera, completed mechanical and seepage tests on the sample. The results show that when the quantity of clay minerals increases, the uniaxial compressive strength, elastic modulus, and rapid crack propagation stress of the weakly cemented rock samples decrease. Initial stress of crack development increases and then decreases, as well as the sample's failure mode changes from shear to tensile. The sample's permeability increases with increasing osmotic and axial pressure differential but decreases with increasing confining pressure under the same amount of clay minerals. The sensitivity of permeability to changes in osmotic pressure differential, axial pressure, and confining pressure increases as the amount of clay minerals increases. The mechanical and seepage characteristics can show significant changes in clay minerals in 20% to 30%.

1. Introduction

Many particular disaster problems have been encountered with the strategic transfer of China's coal resources production center from east to west [1–11]. Weakly cemented rocks have low mechanical strength and poor cementation ability. When the mudstone content is high, the weakly cemented strata will even collapse in water. Weakly cemented rock is prone to fracture and instability of rock stratum under the combined influence of disturbance stress and seepage, resulting in significant engineering disasters such as water and sand inrush [12–14]. It is urgent to understand weakly cemented rock's mechanical properties and seepage characteristics and provide theoretical guidance for practical engineering.

The relevant research results of weakly cemented rocks focus on the basic physical and mechanical properties, seepage characteristics, and micro components [15–31]. The possibility of forecasting the UCS of weakly cemented rocks using their unit weight, P-wave velocity, tensile strength, and elastic modulus was investigated by Wang et al. [32]. Liu et al. performed systematic triaxial compression testing on three typical rock samples from the Ili mining area (mudstone, sandstone, and sandy mudstone) [33]. At the Buertai Coal Mine, Liu et al. collected sandstone from depths of 101.5, 203.2, 317.3, 406.9, 509.9, and 589.8 m. During uniaxial compression experiments, the characteristic strength, acoustic emission (AE), and assessed energy evolution of sandstone were investigated [34]. Under the Brazilian splitting test, Zhao and Liu evaluated the development of the deformation field, acoustic emissions, and energy of four common weakly cemented rocks and discussed the link between the three parameters [35]. Uniaxial compression studies and acoustic emission tests were carried out by Wang et al. on weakly cemented sandstone samples from the Xiaojihan coal mine in Shaanxi Province, China [36].

Weakly cemented rock has the characteristics of deterioration in water. Some scholars have studied the seepage

characteristics of weakly cemented rock [37–42]. Guo et al. created a theoretical model and mathematical relationships to describe the weakening of rock modulus and strength induced by water absorption in the rock substrate. The softening process of water absorption in siltstone specimens was simulated using a theoretical model with low and high fluid pressure as boundary conditions. A uniaxial compression test was also performed on the specimen at various stages of water absorption [43]. Fan et al. studied the seepage mechanism of poorly cemented rock impacted by underground mining operations by collecting Jurassic mudstone and shaly coarse sandstone samples in northern China. Complete stress-strain and postpeak loading and unloading employing seepage experiments under triaxial compression were used to investigate the samples [44]. Liu et al. used X-ray diffraction and triaxial loading tests to investigate the mechanics and permeability of a clay aquiclude. Physical simulation studies investigate the fracturing of the overlying bedrock and aquiclude [45].

Weakly cemented rocks have a wide range and significant differences in mechanical properties. Some scholars study the influence of internal components on the physical and mechanical properties of weakly cemented rocks through statistical analysis [46, 47]. Gupta and Sharma measured several textural characteristics and petrophysical and mechanical properties of quartzites from the lower and upper Himalayas [48]. Based on a complete examination of influencing variables affecting mechanical qualities, Wang et al. established quantitative connections between these sedimentary rocks' petrographic, physical, and mechanical aspects [49]. Zhang et al. developed a weakly cemented water-resisting comparable material based on research of the microstructure and component features of rock strata materials and the similarity in clay mineral concentrations. [50].

Quartz sand, kaolin, and a small amount of cement were used as remolding materials in this paper, and weakly cemented rock samples with clay mineral percentages of 20%, 30%, 40%, 50%, and 60% were created by altering the kaolin content. The effect of clay mineral percentage on mechanical and seepage properties of weakly cemented rock samples is investigated to provide theoretical direction for mitigating geohazards in weakly cemented rock formations in practical engineering.

2. Preparation Steps and Test Schemes

2.1. Preparation Steps. Weakly cemented rocks mainly contain quartz, feldspar, and clay minerals. Quartz and feldspar act as the skeleton particles of the rock, while clay minerals realize the effective binding of the skeleton particles. The amount of clay minerals in weakly cemented rocks varies, as seen in Table 1. According to Meng et al., the average percentage of clay minerals in very weakly cemented rocks is 62%. According to Li et al., the average amount of clay minerals in weakly cemented sandstone is 21%. The chosen proportion of weakly cemented clay minerals is 20%, 30%, 40%, 50%, and 60%, since the actual fraction of weakly cemented rock clay fluctuates between 20 and 60%.

This paper assumes that the skeleton particles are of uniform particle size, and quartz sand of 1400 mesh is taken as the skeleton particles of weakly cemented rock samples. 2000 purpose kaolinite is selected as the clay minerals of the weakly cemented rock samples. As a typical sedimentary rock structure, weakly cemented rocks are generally formed by long-time tectonic stress compression. The remodeling of weakly cemented rock samples in the laboratory is also carried out in compression molding. After extensive tests, it has been found that adding a small amount of silicate cement can be used as a reinforcing agent to accelerate the bonding of the internal components of weakly cemented rocks. 100 g of weakly cemented rock bulk material requires 4 g of silicate cement.

The weakly cemented rock sample prepared in the laboratory goes through five steps: batching, mixing, filling, compression molding, and demoulding, as shown in Figure 1. Firstly, quartz, kaolin, and portland cement bulk materials are weighed according to the set proportion. The second step is to mix all the bulk materials evenly, spray water on the surface of the bulk materials through the watering can, and mix continuously until the mixture is in a water-saturated state. The judgment standard is that the bulk materials are in a small agglomeration state. The third step is to divide the evenly mixed filler into four parts and add them into the die container. After each filling, precompaction shall be carried out by hammering. The sharp cone shall be used to prick and compact the surface before the subsequent filling to make the surface rougher and prevent delamination between fillers at all levels. The fourth step is to place the precompacted stuffing and device on the universal press for pressure to maintain plasticity. The compressive strength of weakly cemented rock samples obtained by compression molding is related to the loading force and holding time selected in the compression molding process. The press's compression molding process is separated into three stages: I, II, and III, with the compaction contact portion, rapid pressure rise section, and constant pressure holding section. The loading process can be set through the built-in program of the press, as shown in Figure 2. The overall strength of the sample is low, and the discrete is substantial when the continuous loading period is set at 30 minutes at the start of the test, but the strength is unchanged when the length is more than 2 hours. The holding duration for all samples is 2 hours to guarantee homogeneity. Finally, the weakly cemented standard rock sample with a diameter of 50 mm and a length of 100 mm is made using the self-designed demoulding table, as illustrated in Figure 3.

The water content W, density ρ, wave velocity P (rounded after averaging), and error variation of the three weakly cemented rock samples at each percentage of cement are shown in Table 2. The variation of water content W, density ρ, and wave velocity P with the clay mineral proportions S is shown in Figures 4, 5, and 6, respectively. The water content of the weakly cemented rock samples increases linearly, and the density and wave velocity decrease linearly with the percentage of clay minerals S increases. Three weakly cemented rock samples with 40% clay

Table 1: Composition proportion of different types of weakly cemented rocks.

Rock type	Average quartz ratio	Average clay minerals ratio	Average feldspar ratio	Paper source
Very weakly cemented rock	26%	62%	12%	Meng et al. [51]
Weakly cemented sandstone	35%	21%	44%	Li et al. [52]

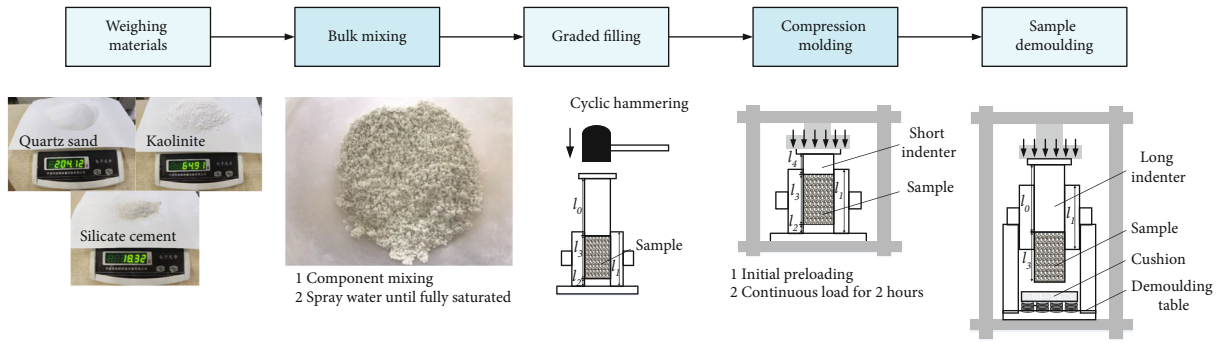

Figure 1: Preparation flow chart of weakly cemented rock sample.

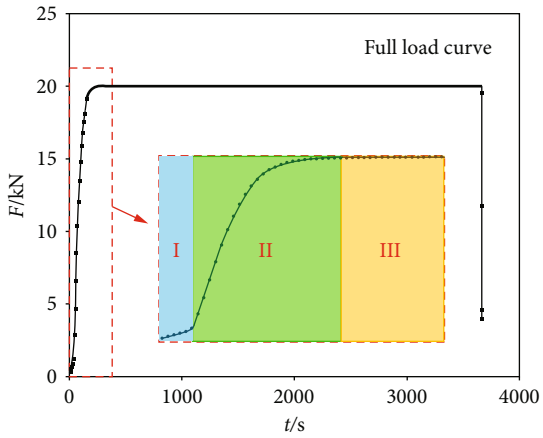

Figure 2: Compression plastic process.

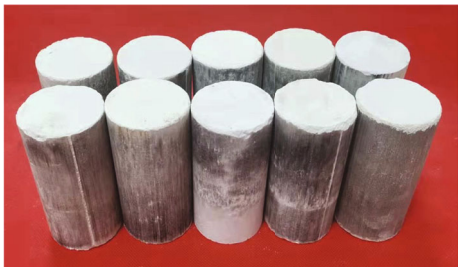

Figure 3: Some weakly cemented rock samples.

minerals were selected for uniaxial compression tests during the preliminary tests to analyze the dispersion of the tests, as shown in Figure 7. Overall, the difference is insignificant, showing that using remolded weakly cemented rock samples allows for a more detailed investigation of the effect of the internal component percentage on the physical and seepage properties of the rock samples.

2.2. Mechanical and Seepage Test Scheme. The uniaxial compression test was carried out with the MTS816 test apparatus on weakly cemented rock samples with 20%, 30%, 40%, 50%, and 60% of clay minerals *S*. The loading rate was 0.3 mm/min with quasistatic displacement loading. During the fracturing phase of the rock sample, two acoustic emission probes were mounted to the loaded specimen in the ring direction to count the frequency of the acoustic emission signal. Scattered spots were sprayed on the outer surface of the specimen to record the macroscopic fracture characteristics of the rock with the help of a high-speed camera, as shown in Figure 8.

Conduct seepage test of weakly cemented rock sample with the help of the self-assembled seepage test device. The pressure vessel and oil and water pressure control device are added based on the uniaxial press, as shown in Figure 9. The main body can be divided into four parts: axial pressure device, circumferential oil pressure control system, osmotic water pressure control system, and flow pressure change monitoring system. The axial pressure device provides stable axial pressure control and monitoring. The oil pressure control system provides stable circumferential pressure control and monitoring. The water pressure control system can provide stable osmotic water pressure. The flow pressure monitoring system uses a pressure gauge and flowmeter. The weighing table and paperless recorder can understand the real-time changes of osmotic pressure difference and flow in seepage and carry out real-time calculations and analysis of permeability.

Considering the diverse compressive strengths of weakly cemented rock samples with different clay mineral proportions, the highest limit of axial loading pressure stated in the permeability test is smaller than the samples' rapid crack propagation stress. Under ultimate bearing, there will be no substantial cracks altering the permeability measurement results in the samples.

It is necessary to guarantee that axial pressure is higher than confining pressure and the osmotic pressure during

Table 2: Changes of average water content W, density ρ, and wave velocity P with clay mineral proportions S.

The clay mineral proportions S (%)	Average moisture content W (%)	Error value (%)	Average density ρ (g/cm^3)	Error value (g/cm^3)	Average wave velocity P (m/s)	Error value (m/s)
20	0.1512	0.00488	2.1973	0.02065	3379	31
30	0.1925	0.00821	2.1306	0.00723	3200	48
40	0.2428	0.00737	2.0487	0.01943	3038	57
50	0.2761	0.00580	1.9910	0.01486	2853	52
60	0.3109	0.00548	1.9125	0.00524	2726	30

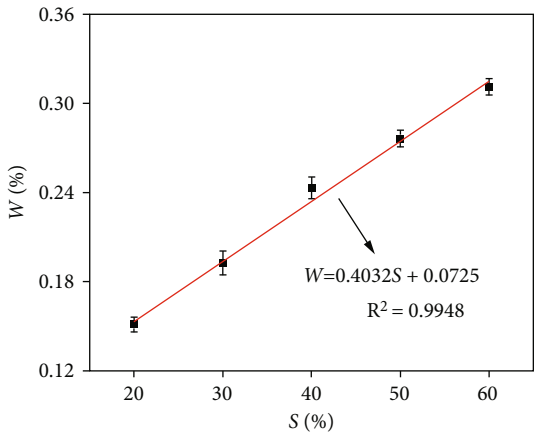

Figure 4: The water content W with S.

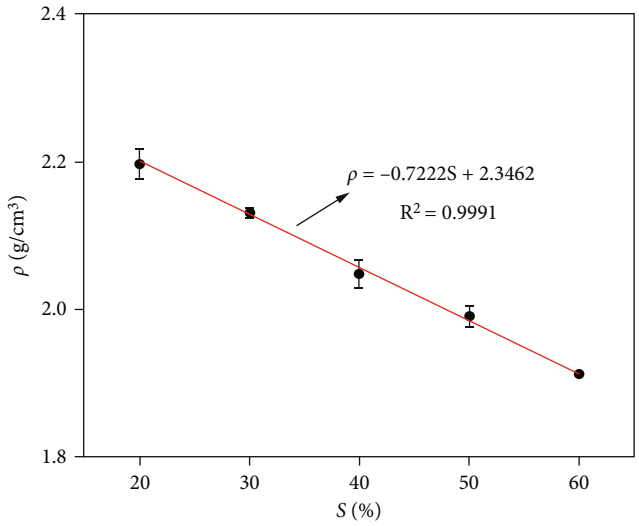

Figure 5: The density ρ with S.

the seepage test. Firstly, set the axial pressure of 2.5 MPa and confining pressure of 2.0 MPa, and carry out the seepage test with an osmotic pressure of 0.8 MPa, 1.0 MPa, 1.2 MPa, 1.4 MPa, and 1.6 MPa successively, measure the test data of stable seepage for 20 min, calculate the average permeability, and analyze the variation law of permeability with osmotic pressure. Secondly, the confining pressure and osmotic pressure remain unchanged, and the seepage test under an axial pressure of 2.5 MPa, 3.0 MPa, 3.5 MPa, 4.0 MPa, and 4.5 MPa is carried out successively to analyze the variation law of permeability with axial pressure. Finally, the axial pressure and osmotic pressure remain unchanged, and the seepage test under confining pressure of 2.0 MPa, 2.5 MPa, 3.0 MPa, 3.5 MPa, and 4.0 MPa is carried out successively to analyze the variation law of permeability with confining pressure.

3. Analysis of Mechanical Properties

3.1. Mechanical Characteristic Parameters. Figure 10 shows the relationship between the stress-strain curve and acoustic emission frequency signal when the proportion of clay minerals is 20%. The constant coordinate selects the loading time as the variable. The black line is the change curve of stress with time, the blue line is the change curve of acoustic emission frequency with time, and the red line is the change curve of acoustic emission cumulative frequency with time. The AE signal will increase significantly near the peak stress, indicating that the AE frequency signal collected at the peak stress will increase significantly because much derivative propagation of cracks exceeds the ultimate bearing capacity of weakly cemented rock samples. Unlike the conventional brittle rock, the weakly cemented rock sample will not appear in the overall instability failure caused by rapid fracture after reaching the peak stress. After the peak, it can still bear a certain load, but the load strength will gradually decrease with the continuous loading, showing significant compressive plastic characteristics.

By combining acoustic emission characteristics and stress time history curve, the whole failure process of weak cementation can be divided into the stable elastic stage I, crack incubation stage II, crack rapid expansion stage III, and overall failure stage IV [36]. The stable elastic stage is from the start time to the slope inflection point b. The crack preparation section is from the slope inflection point b to the first two double slope intersections c. The crack rapid expansion section is from the first two double slope intersections c to the last two slope intersections e, and the instability stage is from the previous two slope intersections e to the loading endpoint. This division method can divide the traditional elastic modulus into two parts. One part is the real elastic deformation section. In this part, all pores are closed in stable compaction and produce fewer acoustic emission signals. In this stage, the pressure is eliminated to completely restore the deformation. The other part is the expansion of some fractures caused by pressure. The expansion rate of this part is relatively low, which will not cause significant damage to

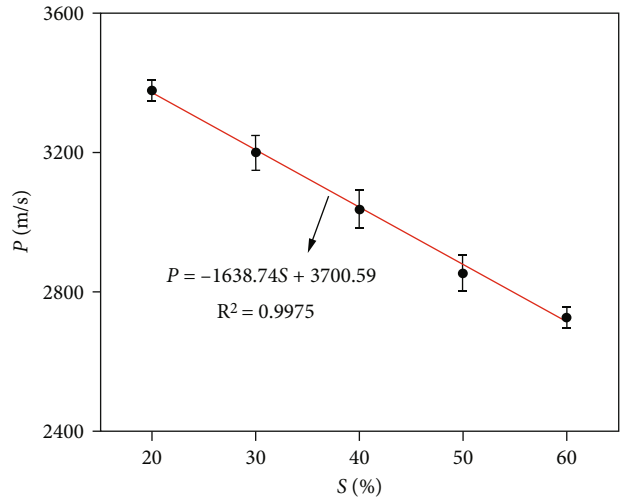

Figure 6: The wave velocity P with S.

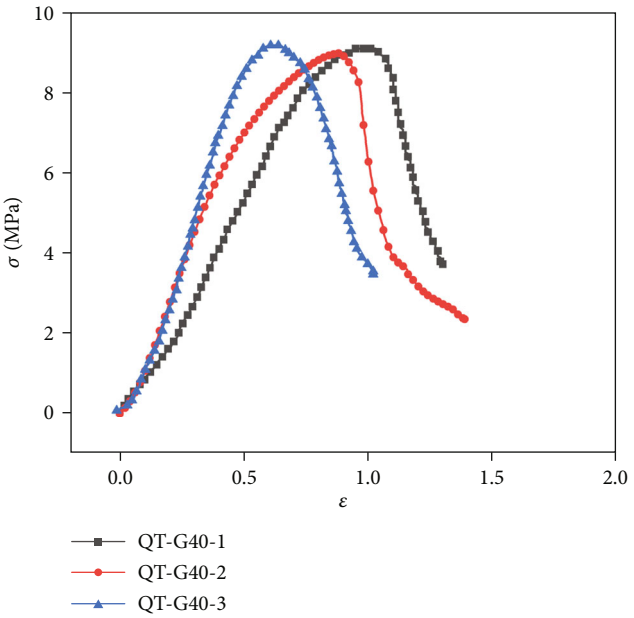

Figure 7: Stress-strain curve of uniaxial compression.

the rock sample, and the overall acoustic emission signal is relatively small. Many small damages in the rock sample are not fully reflected in the macro mechanical characteristics. Unlike conventional brittle rock, when the weakly cemented rock sample enters the unloading stage, the accumulated internal damage will not disappear completely. Combined with the acoustic emission cumulative frequency signal, it can help the weakly cemented rock sample find the endpoint of the elastic stage and effectively identify the characteristic points of the stress-strain curve. Unlike the direct reduction of the brittle rock failure stage, the plastic deformation stage of weakly cemented rock is more prolonged. It is more accurate to redefine the stress-strain curve by acoustic emission characteristics.

After experiencing a stable crack, the rapid crack propagation stress describes the stress when the sample experiences rapid and unstable crack growth. The steady crack growth stage and the quick crack growth stage are assumed to be part of the elastic stage's overall process. The differences in fracture shape and size in the sample will produce random failure characteristics after the quick crack growth stage. Using the rapid crack propagation stress instead of the peak stress is a superior technique for avoiding engineering disasters.

According to the above classification characteristics, the acoustic emission stress comprehensive analysis curves with clay mineral proportions of 30%, 40%, 50%, and 60% are selected. As illustrated in Figure 11, the stress-time curves of weakly cemented rock with various clay mineral contents are summarized and analyzed. The maximum compressive strength of weakly cemented rocks gradually decreases with the increase of clay minerals. The elastic modulus gradually decreases, but the difference in peak strain is small. The changes of peak stress σ_p, initial stress of crack development σ_1, rapid crack propagation stress σ_2, elastic modulus E, and peak strain ε_p with the clay mineral proportions S are counted. The data are shown in Table 3. Draw the peak stress and elastic modulus fluctuation curve with the proportion of clay minerals as indicated in Figure 12. Peak stress decreases linearly from 13.683 MPa to 5.438 MPa when the percentage of clay minerals increases from 20% to 60%. The elastic modulus decreases nonlinearly with the increase in the proportion of clay minerals. The speed of elastic modulus decline is significantly higher when the percentage of clay minerals is low than when the amount of clay minerals is high.

Figure 13 shows the curves of the initial stress of crack development σ_1 and the rapid crack propagation stress σ_2 with the clay mineral proportions S. The initial stress of rapid crack growth decreases linearly with the increase of clay mineral proportion. In contrast, when the amount of clay minerals increases, the initial stress of crack development increases initially, then reduces. Peak stress, elastic modulus, and initial stress of rapid crack growth indicate that the overall strength of the sample decreases gradually with the increase of clay mineral proportion, but combined with the various characteristics of initial stress of crack development, it shows that there is an optimal ratio between clay minerals and skeleton particles. When the proportion of clay minerals is small, there is no clay mineral cementation between skeleton particles, and crack expansion will occur under minimal pressure. When the proportion of clay minerals is high, the lack of support of skeleton particles will lead to deformation and crack development. When the amount of clay minerals in weakly cemented rock samples is 30%, the initial crack development stress is highest. There is a substantial difference when the proportion of clay minerals ranges from 20% to 30%.

3.2. Macroscopic and Microscopic Failure Characteristics. Figure 14 shows the fracture characteristics of weakly cemented rock samples with different clay minerals after uniaxial compression. With the increase in the proportion

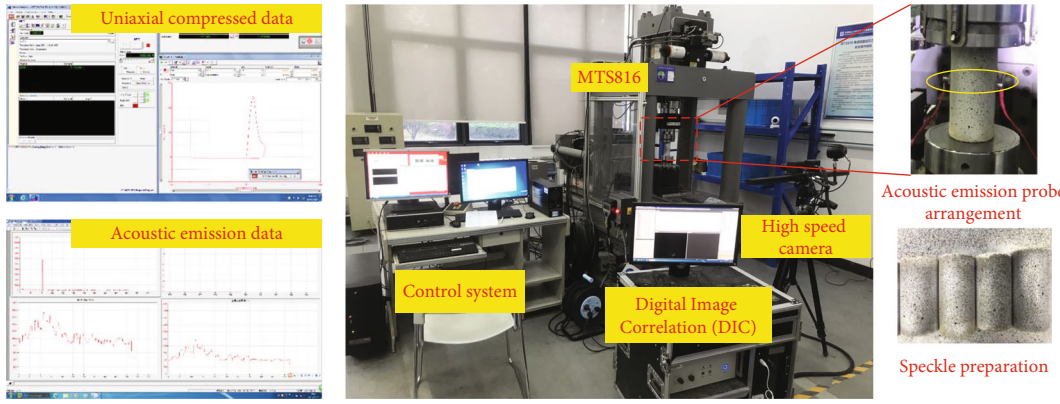

Figure 8: Uniaxial compression test system of weakly cemented rock sample.

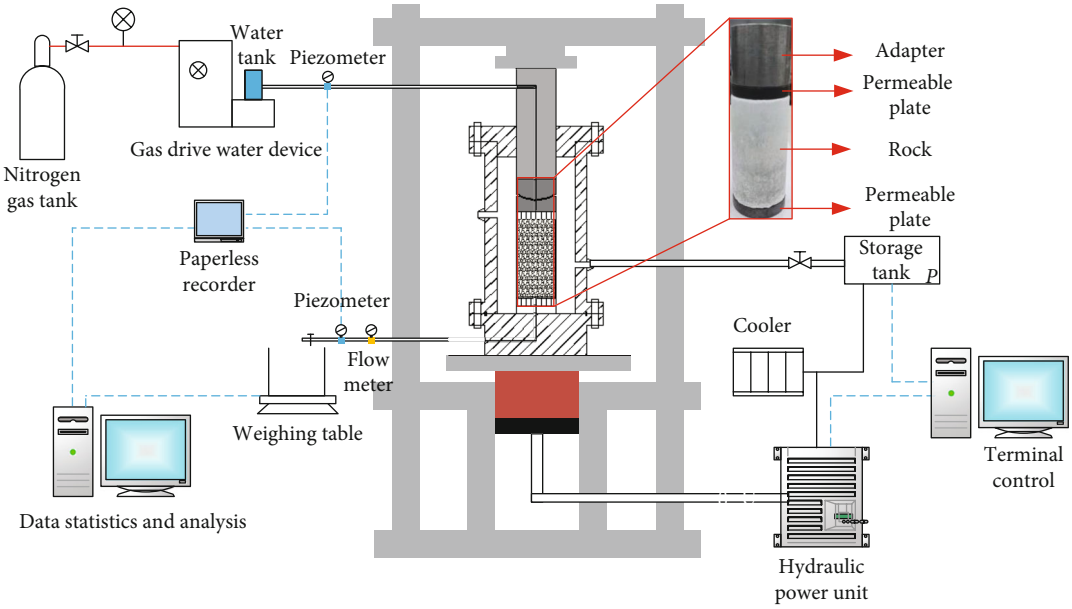

Figure 9: Seepage test system for weakly cemented rock samples.

of clay minerals, the crack of weakly cemented rock samples gradually evolved from oblique penetration mode to vertical penetration mode. According to this analysis, the failure mechanism of weakly cemented rock changed from shear to tensile failure mode as the clay mineral proportions increased.

Figure 15 shows the main strain nephogram of the crack development process of weakly cemented rock sample when the proportion of clay minerals is 20% and 60% by a high-speed camera. When the proportion of clay minerals is 20%, a sizeable inclined crack will appear in the weakly cemented rock sample after reaching the peak stress. With the continuous action of load, the crack will continue to expand along the inclined direction, gradually form a strain concentration area in the central area of the rock sample, and then, a large crack will appear and continue to increase the range of strain concentration area until the inclined crack runs through the whole sample. When the proportion of clay minerals is 60%, the weakly cemented rock sample will have a main crack of vertical tension failure and a secondary crack next to it after reaching the peak stress. With the continuous action of load, the crack will gradually expand to the bottom of the rock sample, the opening of the upper crack will continue to increase, and the derived secondary crack will gradually converge with the main crack to accelerate the damage to the rock sample. The preferential expansion area of the initial crack is located in the tensile crack area at the top. The secondary crack meets with the main crack, with the continuous downward movement of the maximum principal strain concentration area. The preferential development area of the crack turns to the lower crack expansion area, and the depth and range continue to increase until the inclined crack runs through the whole sample.

20% and 60% of the clay minerals proportions are analyzed by SEM, as shown in Figure 16. At 20% of the clay minerals, large-sized quartz is observed as the skeleton particles, with a small amount of kaolinite clay minerals

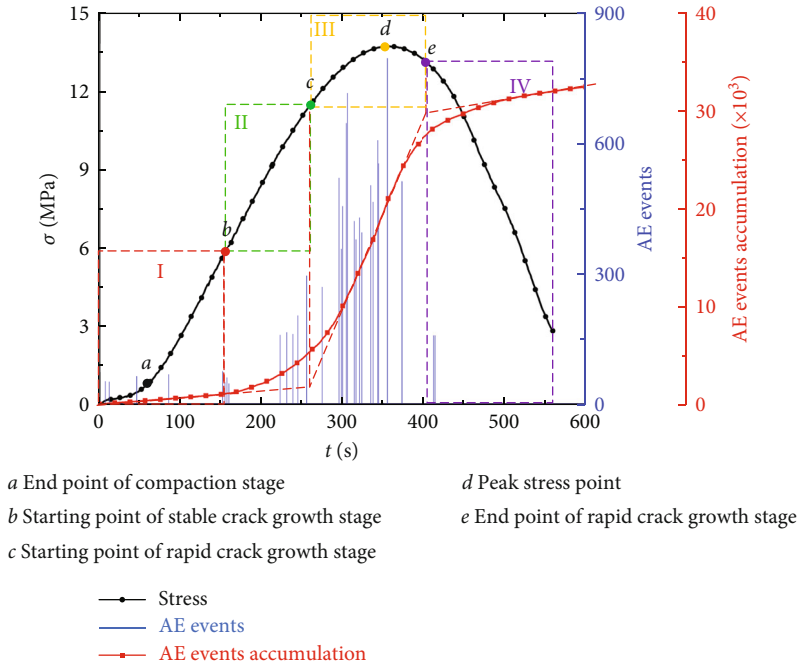

Figure 10: Comparative analysis of stress and acoustic emission signals with $S = 20\%$.

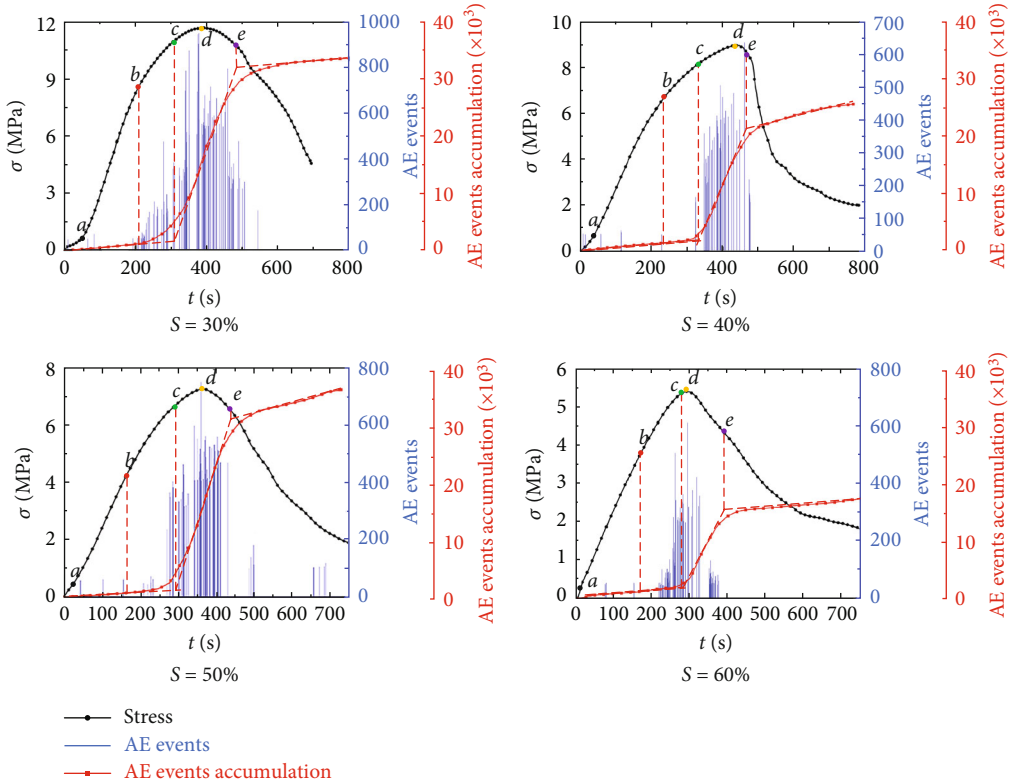

Figure 11: Comparative analysis of stress and acoustic emission signals under the different proportion of clay minerals.

attached to the surface of the skeleton particles. And fissures are visible in the microstructure with a maximum width of 6 μm. At 60% of the clay minerals, no significant skeleton particles can be seen in the microstructure, and only clusters of clay minerals are observed. It can be found that when the percentage of clay minerals is high, the overall porosity is more significant, and the internal particles are more loosely distributed but more uniformly distributed. As the clay

Table 3: Mechanical characteristic parameters of weakly cemented rock samples.

The clay mineral proportions S(%)	20	30	40	50	60
Peak stress σ_p (MPa)	13.683	11.662	8.991	7.272	5.438
Initial stress of crack development σ_1 (MPa)	5.725	8.826	6.796	4.262	3.742
Rapid crack propagation stress σ_2 (MPa)	11.526	10.732	8.124	6.638	5.291
Peak strain ε_p (%)	0.707	0.763	0.876	0.731	0.586
Elastic module E (GPa)	2.788	2.247	1.633	1.343	1.079

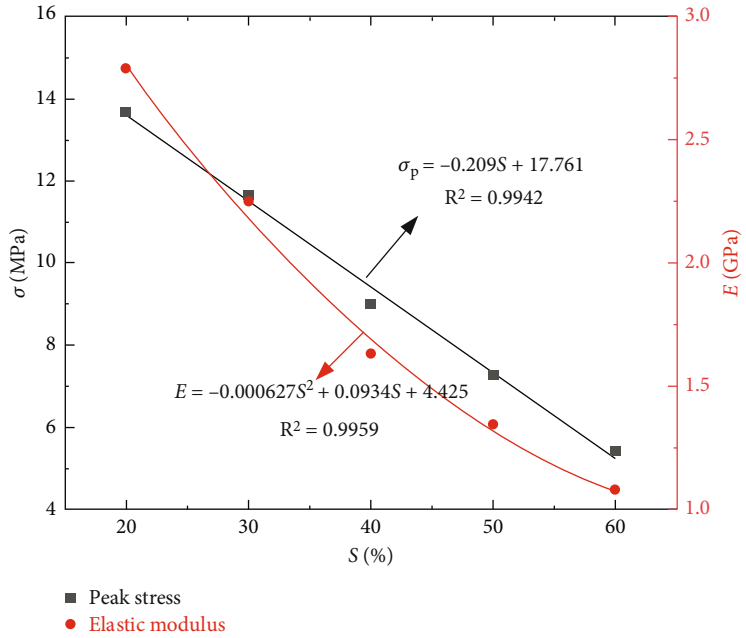

Figure 12: Variation of the peak stress and elastic modulus.

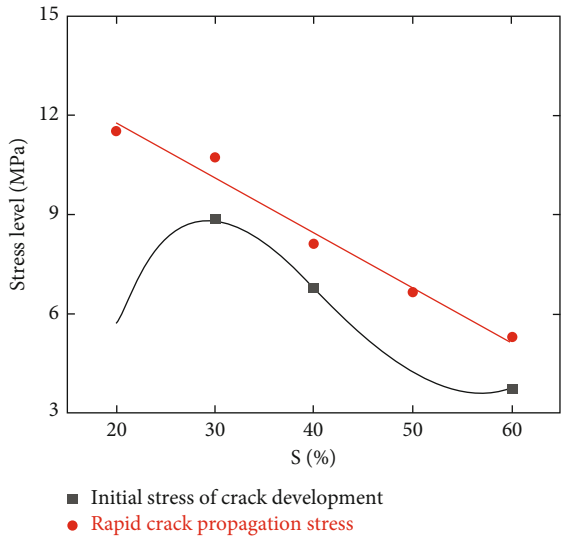

Figure 13: Variation of initial stress of crack development and rapid crack propagation stress.

minerals are more water-absorbent, the general water content increases accordingly. When subjected to pressure, the overall specimen will be damaged due to the loss of adhesion between the clay minerals. And the damage pattern is expressed as tensile damage. When the clay minerals are minor, there are more initial microfractures due to the random distribution of quartz, and a more prolonged compression phase is observed in the uniaxial compression process. Still, the strength of the quartz skeleton particles is greater, which increases the strength of the whole sample.

The change of crack propagation mode and micromorphology can explain the change law of mechanical parameters to a certain extent. When the proportion of clay minerals is relatively low, the initial porosity is large, and there will be a significant compaction stage. Due to many skeleton particles, the overall strength is high, and the need for significant interlayer dislocation to induce overall shear failure and the rapid expansion stress is relatively high. When the proportion of clay minerals is relatively high, the initial porosity is relatively small, and the compaction stage is not apparent. Because the primary failure mode is a tensile failure between clay minerals, the overall strength and rapid expansion stress are relatively small.

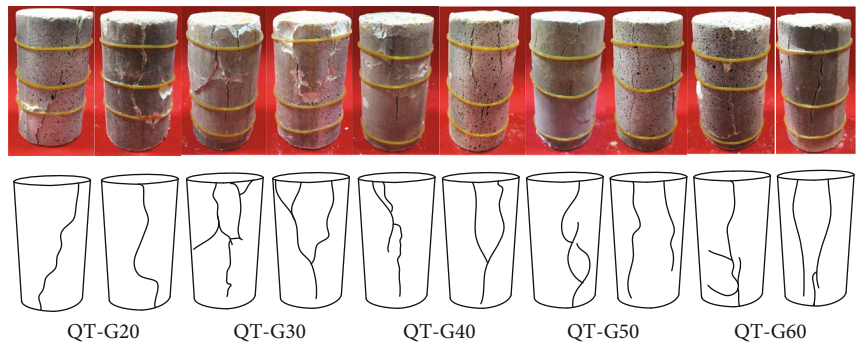

Figure 14: Failure characteristics of weakly cemented rock samples with different clay minerals.

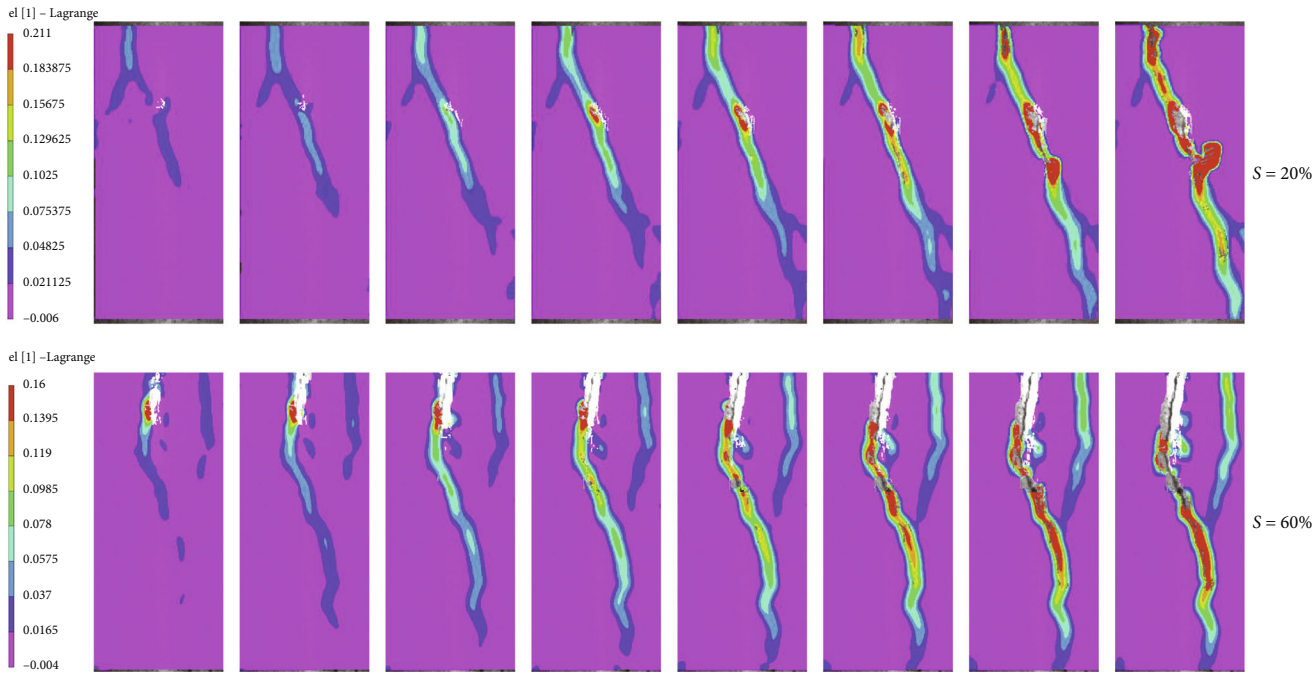

Figure 15: main strain nephogram of the crack development process with $S = 20\%$ and $S = 60\%$.

When the proportion of clay minerals is small, the initial crack between clay minerals and skeleton particles is significant. After the compaction stage, the initial crack expansion can occur only with a small load. With the increase in the proportion of clay minerals, the initial crack between clay minerals and skeleton particles gradually decreases, and the initial crack expansion stress increases. However, with the further increase in the proportion of clay minerals, the initial crack expansion occurs between clay minerals. As the proportion of skeleton particles decreases, the initial crack development stress will gradually decrease due to uneven load conduction.

4. Seepage Characterization

With the aid of a self-assembled percolation test system, the steady-state method was used to calculate the variation of the average permeability k with permeability, axial pressure, and circumferential pressure for different clay mineral percentages, calculated as

$$k = \frac{Q\mu L}{A(P_1 - P_2)}, \tag{1}$$

where k is rock permeability, m^2; Q is the unit flow, m^3/s; μ is the dynamic viscosity, Pa·s; L is the length of the sample, m; A is the cross-sectional area of the sample,m^2; and $P_1 - P_2$ is the seepage pressure, MPa. During the test, one side is connected to the atmosphere, and the other is connected to the pressure head. Under stable conditions, the pressure of the connected head is taken as the pressure difference. Later, P_s is simplified to represent the osmotic pressure. The permeability of the weakly cemented rock samples analyzed in this work is high, as evaluated using steady-state methods. The average permeability can be determined to reduce error.

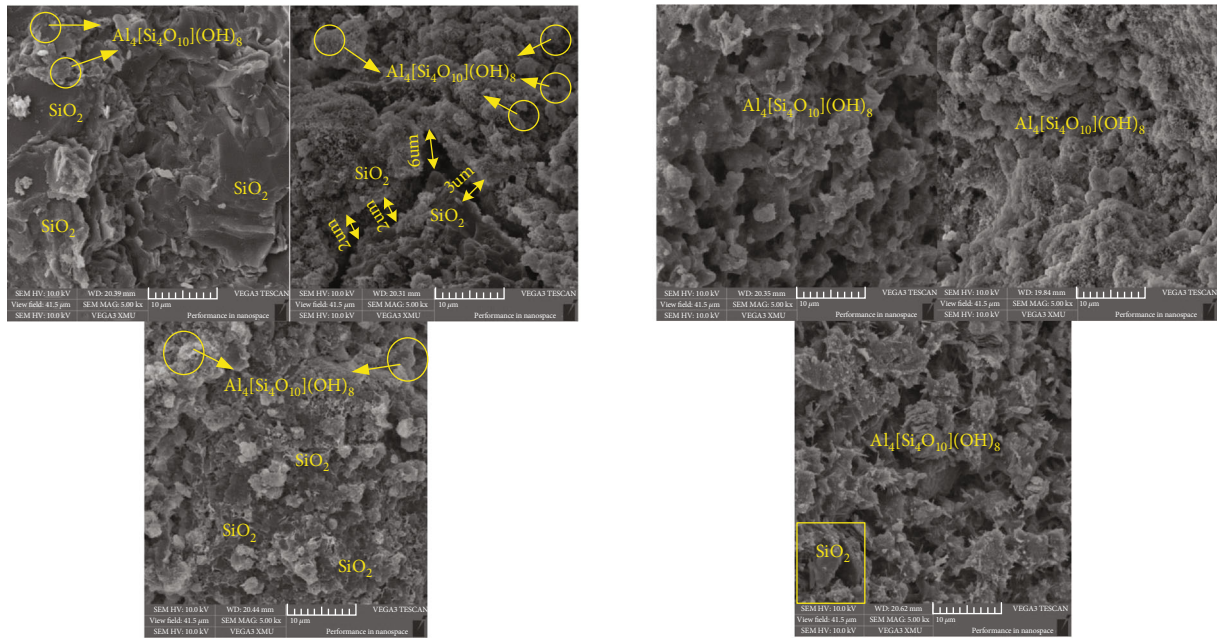

Figure 16: Microstructure of fragments with $S = 20\%$ and $S = 60\%$.

Table 4: Variation of permeability k with osmotic pressure P_s under different clay mineral proportions S.

P_s (MPa)	k (m^2)				
	20%	30%	40%	50%	60%
0.8	3.1314E-14	7.9000E-15	4.4714E-15	2.5667E-15	2.1604E-15
1.0	3.6169E-14	9.3600E-15	4.9143E-15	2.9667E-15	2.7114E-15
1.2	4.3658E-14	9.9300E-15	5.4200E-15	3.5444E-15	3.3399E-15
1.4	5.0200E-14	1.1800E-14	6.2857E-15	4.1267E-15	3.9364E-15
1.6	5.3400E-14	1.4080E-14	7.6429E-15	5.0222E-15	4.1739E-15

4.1. Variation of Permeability with Osmotic Pressure. Table 4 shows the data table of the variation of permeability k with osmotic pressure P_s for different clay mineral occupation ratios S. Figure 17 shows the surface plot of the variation of permeability k with osmotic pressure P_s for different clay mineral occupations ratios S. Under the same clay mineral proportion S, the permeability k increased linearly with the increased osmotic pressure P_s. With the increase of clay mineral proportion S, the permeability incremental quantity gradually increased with the increase of osmotic pressure P_s. The maximum increase occurred at a clay mineral proportion of 50%. The permeability k increased from 2.567E-15 m^2 to 5.022E-15 m^2, increasing 95.67%. Under the same osmotic pressure P_s, the permeability k decreases gradually with the increase of the clay mineral proportion S. The overall decrease is the same at all seepage pressures, with the maximum reduction occurring when the clay mineral proportion changes from 20% to 30%. The most significant decrease occurs at osmotic pressure of 0.8 MPa, where the permeability k decreases from 3.131E-14 m^2 to 2.160E-15 m^2, decreasing 93.10%. The sensitivity of permeability to osmotic pressure is defined as the increase in permeability under various osmotic pressures compared to the initial osmotic pressure. Similarly, the increase of permeability under different clay mineral proportions relative to 20% clay proportion is used to characterize the sensitivity of permeability with clay mineral proportion. The combined analysis revealed that the sensitivity of permeability k to changes in osmotic pressure P_s increased as the clay mineral proportions increased. As the osmotic pressure P_s increases, the sensitivity of permeability k to changes in the clay mineral proportions gradually decreases.

4.2. Variation of Permeability with Axial Pressure. Table 5 shows the various data of permeability k with axial pressure P_a under different clay mineral proportions S. Figure 18 shows the variation curve of permeability k with axial pressure P_a under clay mineral proportion S. Under the same clay mineral proportion S, the permeability k increases monotonically with the increase of axial pressure P_a. When the proportion of clay minerals S is higher, the permeability incremental quantity rapidly increases with increasing axial pressure P_a. The maximum increase occurs when the proportion of clay minerals S is 50%, and the permeability k increases from 5.022E-15 m^2 to 1.406E-14 m^2, increasing 179.99%. Under the same axial pressure P_a, the permeability

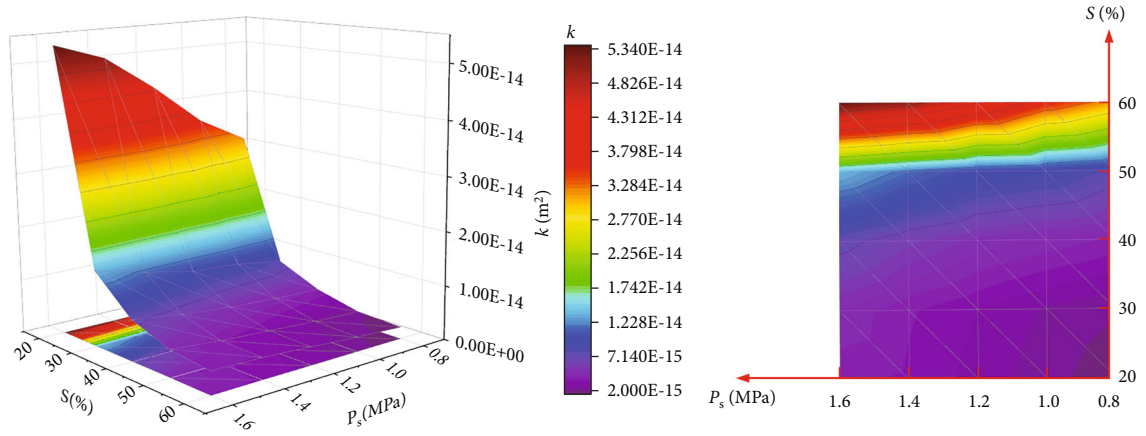

Figure 17: Variation surface of permeability k with osmotic pressure P_s under different clay mineral proportions S.

Table 5: Variation of permeability k with axial pressure P_a under different clay mineral proportions S.

P_a (MPa)	k (m^2)				
	20%	30%	40%	50%	60%
2.5	5.3400E-14	1.4080E-14	7.6429E-15	5.0222E-15	4.1739E-15
3.0	5.5812E-14	1.6298E-14	9.3781E-15	6.4570E-15	5.2777E-15
3.5	5.8204E-14	1.8679E-14	1.1821E-14	9.0199E-15	6.7061E-15
4.0	6.0567E-14	2.1699E-14	1.4708E-14	1.0862E-14	8.1183E-15
4.5	6.3231E-14	2.4733E-14	1.7116E-14	1.4062E-14	1.0519E-14

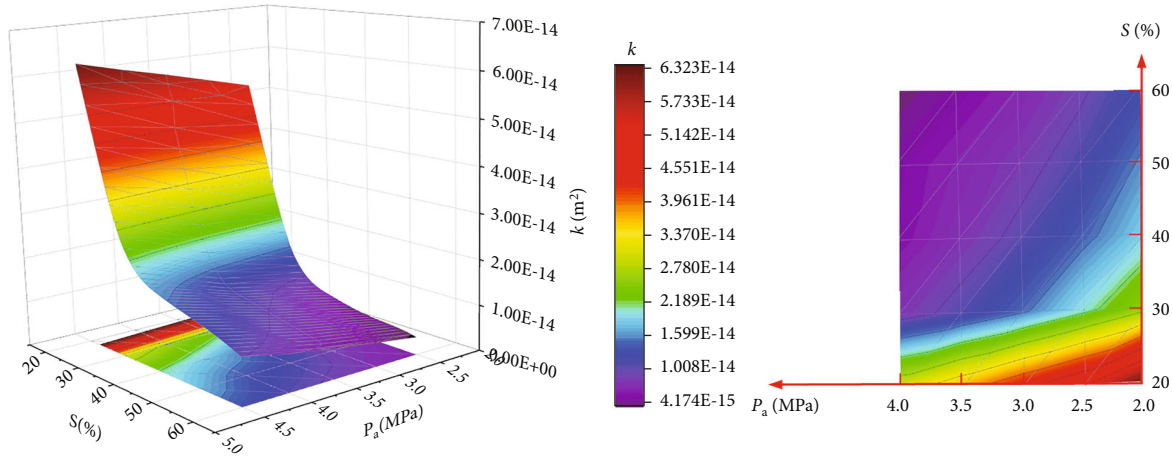

Figure 18: Variation surface of permeability k with axial pressure P_a under different clay mineral proportions S.

k decreases gradually with the increase of clay mineral proportion S. With the increase of axial pressure P_a, the decrease of permeability k decreases slowly, and the maximum decrease occurs when the proportion of clay minerals changes from 20% to 30%. The maximum decrease occurs when the axial pressure P_a is 2.5 MPa, and the permeability k decreases from 5.340E-14 m^2 to 4.173E-15 m^2, decreasing 92.18%. Comprehensive analysis shows that with the increase of clay mineral proportion S, the sensitivity of permeability k with axial pressure P_a increases. With the increase of axial pressure P_a, the sensitivity of permeability k with the proportion of clay minerals S decreases.

4.3. Variation of Permeability with Confining Pressure. Table 6 shows the various data of permeability k with axial confining pressure P_c under different clay mineral proportions S. Figure 19 shows the variation curve of permeability k with confining pressure P_c under clay mineral proportion S. With the same clay mineral fraction proportion S, the permeability k progressively decreases as the confining pressure P_c rises. With the increase of the percentage of clay minerals S, the permeability incremental quantity gradually decreases as the confining pressure P_c rises. The maximum decrease occurs when the percentage of clay minerals S is 60%, and the permeability k decreases from 1.052E-14 m^2 to 1.088E-

Table 6: Variation of permeability k with confining pressure P_c under different clay mineral proportions S.

P_c (MPa)	k (m^2)				
	20%	30%	40%	50%	60%
2.0	6.3231E-14	2.4733E-14	1.7116E-14	1.4062E-14	1.0519E-14
2.5	5.0289E-14	1.8521E-14	1.2458E-14	9.1052E-15	6.6548E-15
3.0	4.3587E-14	1.2984E-14	8.3540E-15	6.0029E-15	4.3215E-15
3.5	3.6854E-14	8.7215E-15	5.2685E-15	4.3824E-15	2.5486E-15
4.0	3.0554E-14	5.5495E-15	3.0882E-15	2.6878E-15	1.0876E-15

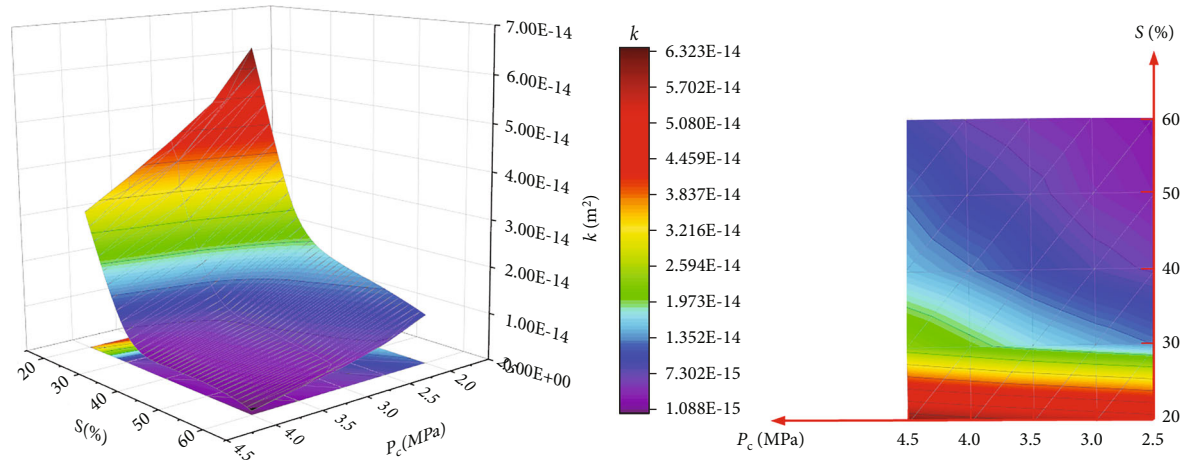

Figure 19: Variation surface of permeability k with confining pressure P_c under different clay mineral proportions S.

15 m^2, decreasing 89.66%. Under the same confining pressure P_c, the permeability k gradually decreases with the increase of the percentage of clay minerals S. With the increase of the confining pressure P_c, the decrease in permeability k gradually increases with the increase of the surrounding pressure P_c. The maximum decrease occurs when the percentage of clay minerals S changes from 20% to 30%. The maximum overall decrease in permeability k occurs at an envelope pressure of 4.0 MPa, when the permeability k decreases from 3.055E-14 m^2 to 1.088E-15 m^2, decreasing 96.44%. The combined analysis reveals that the sensitivity of permeability k to changes in the confining pressure P_c increases as the percentage of clay minerals S increases. With the increase of confining pressure P_c, the sensitivity of permeability k increases with the proportion of clay minerals S increases.

5. Discussion

The traditional remolding is applied to the soil. Based on the remolding of weakly cemented rock powder by Meng et al., a new device is designed for weakly cemented remolding. Compared with Meng et al. remolded weakly cemented rock with a single component, this paper considered the influence of the different proportions of clay minerals. It can have a more comprehensive understanding of the weakly cemented rock's mechanical properties and seepage characteristics. When mechanical and seepage tests of weakly cemented rock are combined, it is discovered that the mechanical properties and seepage characteristics alter the most when the proportion of clay minerals is between 20% and 30%. The initial crack propagation stress is considerably lowered, the permeability is significantly raised, and seepage stability is more likely to occur if the fraction of clay minerals in the weakly cemented rock layer is reduced from 30% to 20% due to the influence of seepage in the project. In order to prevent geological disasters, it is vital to concentrate on the weakly cemented rock strata with clay minerals accounting for 20% to 30% of the total. However, seepage erosion has not been thoroughly investigated, and seepage erosion of remolded fractured rock mass will be investigated in the future.

6. Conclusion

The mechanical and percolation properties of weakly cemented rock samples with 20%, 30%, 40%, 50%, and 60% clay minerals, respectively, are investigated in this paper, with the following primary findings:

(1) The uniaxial compressive strength of weakly cemented rocks tends to fall linearly as clay minerals increase, with a more dramatic expression in the compression-density stage. The modulus of elasticity displays a nonlinear falling pattern with relatively slight variations in peak strain. The rapid crack propagation stress extension decreased about

linearly. The initial stress of crack development tended from increase to decrease

(2) The large-sized quartz microstructure has many microfractures. When the amount of clay minerals is 20%. it prolongs the loading compression phase and generates shear damage throughout the specimen. The breakdown of adhesion between the clay minerals causes tensile damage across the specimen when the amount of clay minerals is 60%

(3) Under the same clay mineral proportion, the permeability increases gradually with rising permeability and axial pressure. Moreover, it drops slowly with increasing circumferential pressure. Permeability becomes more sensitive to changes in osmotic pressure, axial pressure, and confining pressure as the clay mineral proportion increases. The sensitivity of permeability to clay mineral percentage diminishes as osmotic and axial pressure rise. The permeability with clay mineral percentage becomes more sensitive as confining pressure rises

Data Availability

The data used to support the findings of this study are available from the corresponding author upon request.

Conflicts of Interest

The authors declare that there is no conflict of interest regarding the publication of this paper.

Authors' Contributions

Shiru Guo is the submitting author.

Acknowledgments

This work was supported by the National Natural Science Foundation of China (51974296, 52061135111, and 52074240).

References

[1] H. Gui, R. Hu, H. Zhao et al., "Overview of surface water hazards in China coalmines," *Water Practice and Technology*, vol. 14, no. 4, pp. 851–862, 2019.

[2] L. Fan and X. Ma, "A review on investigation of water-preserved coal mining in western China," *International Journal of Coal Science & Technology*, vol. 5, no. 4, pp. 411–416, 2018.

[3] H. Gui, H. Qiu, Z. Chen, P. Ding, H. Zhao, and J. Li, "An overview of surface water hazards in China coal mines and disaster-causing mechanism," *Arabian Journal of Geosciences*, vol. 13, no. 2, 2020.

[4] W. Yang and X. Xia, "Study on mining failure law of the weak and weathered composite roof in a thin bedrock working face," *Journal of Geophysics and Engineering*, vol. 15, no. 6, pp. 2370–2377, 2018.

[5] H. Li, B. Zhang, H. Bai et al., "Surface water resource protection in a mining process under varying strata thickness—a case study of Buliangou Coal Mine, China," *China. Sustainability*, vol. 10, no. 12, p. 4634, 2018.

[6] Z. Dou, Y. M. Liu, X. Y. Zhang et al., "Influence of layer transition zone on rainfall-induced instability of multilayered slope," *Lithosphere*, vol. 2021, no. 4, p. 2277284, 2021.

[7] G. Li, Y. Hu, and T. Sm, "Analysis of deformation control mechanism of prestressed anchor on jointed soft rock in large cross-section tunnel," *Bulletin of Engineering Geology and the Environment*, vol. 80, no. 12, pp. 9089–9103, 2021.

[8] C. Zhu, M. Karakus, M. C. He et al., "Volumetric deformation and damage evolution of Tibet interbedded skarn under multistage constant-amplitude-cyclic loading," *International Journal of Rock Mechanics and Mining Sciences*, vol. 152, p. 105066, 2022.

[9] P. Zhang, D. F. Zhang, Y. Yang et al., "A case study on integrated modeling of spatial information of a complex geological body," *Lithosphere*, vol. 2022, no. 10, p. 2918401, 2022.

[10] X. S. Li, Q. H. Li, Y. J. Hu et al., "Study on Three-Dimensional Dynamic Stability of Open-Pit High Slope under Blasting Vibration," *Lithosphere*, vol. 2022, article 6426550, p. 17, 2022.

[11] Q. Wang, M. C. He, S. C. Li et al., "Comparative study of model tests on automatically formed roadway and gob-side entry driving in deep coal mines," *International Journal of Mining Science and Technology.*, vol. 31, no. 4, pp. 591–601, 2021.

[12] G. Fan, D. Zhang, S. Zhang, and C. Zhang, "Assessment and prevention of water and sand inrush associated with coal mining under a water-filled buried gully: a case study," *Mine Water and the Environment*, vol. 37, no. 3, pp. 565–576, 2018.

[13] H. Li, J. Li, L. Li, H. Xu, and J. Wei, "Prevention of water and sand inrush during mining of extremely thick coal seams under unconsolidated Cenozoic alluvium," *Bulletin of Engineering Geology and the Environment*, vol. 79, no. 6, pp. 3271–3283, 2020.

[14] Y. Xu, Y. Luo, J. Li, K. Li, and X. Cao, "Water and sand inrush during mining under thick unconsolidated layers and thin bedrock in the Zhaogu No. 1 Coal Mine, China," *Mine Water and the Environment*, vol. 37, no. 2, pp. 336–345, 2018.

[15] T. Zhu, W. Li, Q. Wang, and Y. Hu, "Engineering geological and petrological characterization of paleoweathered rock in the K1/J2 contact zone in the Ordos Basin, China," *Environmental Earth Sciences*, vol. 81, no. 6, p. 81, 2022.

[16] R. Hebib, D. Belhai, and B. Alloul, "Estimation of uniaxial compressive strength of North Algeria sedimentary rocks using density, porosity, and Schmidt hardness," *Arabian Journal of Geosciences*, vol. 10, no. 17, 2017.

[17] W. Yu, K. Li, Z. Liu, B. An, P. Wang, and H. Wu, "Mechanical characteristics and deformation control of surrounding rock in weakly cemented siltstone," *Environmental Earth Sciences*, vol. 80, no. 9, 2021.

[18] B. Minaeian and K. Ahangari, "Prediction of the uniaxial compressive strength and Brazilian tensile strength of weak conglomerate," *International Journal of Geo-Engineering*, vol. 8, no. 1, 2017.

[19] N. Sabatakakis, G. Tsiambaos, S. Ktena, and S. Bouboukas, "The effect of microstructure on mi strength parameter variation of common rock types," *Bulletin of Engineering Geology and the Environment*, vol. 77, no. 4, pp. 1673–1688, 2018.

[20] H. Niu, J. Wei, H. Yin, D. Xie, and W. Zhang, "An improved model to predict the water-inrush risk from an Ordovician limestone aquifer under coal seams: a case study of the Longgu coal mine in China," *Carbonates and Evaporites*, vol. 35, no. 3, 2020.

[21] J. Moon and S. Jeong, "Effect of highly pervious geological features on ground-water flow into a tunnel," *Engineering Geology*, vol. 117, no. 3-4, pp. 207–216, 2011.

[22] G. Zhang, W. Zhang, C. Wang, G. Zhu, and B. Li, "Mining thick coal seams under thin bedrock–deformation and failure of overlying strata and alluvium," *Geotechnical and Geological Engineering*, vol. 34, no. 5, pp. 1553–1563, 2016.

[23] M. Z. Gao, J. Xie, J. Guo, Y. Q. Lu, Z. Q. He, and C. Li, "Fractal evolution and connectivity characteristics of mining-induced crack networks in coal masses at different depths," *Geomechanics and Geophysics for Geo-Energy and Geo-Resources*, vol. 7, no. 1, p. 9, 2021.

[24] Y. Wang, H. N. Yang, J. Q. Han, and C. Zhu, "Effect of rock bridge length on fracture and damage modelling in granite containing hole and fissures under cyclic uniaxial increasing-amplitude decreasing-frequency (CUIADF) loads," *International Journal of Fatigue*, vol. 158, article 106741, 2022.

[25] L. Chen, X. Feng, D. Xu, W. Zeng, and Z. Zheng, "Prediction of water inrush areas under an unconsolidated, confined aquifer: the application of multi-information superposition based on GIS and AHP in the Qidong coal mine, China," *Mine Water and the Environment*, vol. 37, no. 4, pp. 786–795, 2018.

[26] Y. Q. Su, F. Q. Gong, S. Luo, and Z. X. Liu, "Experimental study on energy storage and dissipation characteristics of granite under two-dimensional compression with constant confining pressure," *Journal of Central South University*, vol. 28, no. 3, pp. 848–865, 2021.

[27] Z. J. Wu, Z. Y. Wang, L. F. Fan, L. Weng, and Q. S. Liu, "Micro-failure process and failure mechanism of brittle rock under uniaxial compression using continuous real-time wave velocity measurement," *Journal of Central South University*, vol. 28, no. 2, pp. 556–571, 2021.

[28] D. Chen, H. Chen, W. Zhang, J. Lou, and B. Shan, "An analytical solution of equivalent elastic modulus considering confining stress and its variables sensitivity analysis for fractured rock masses," *Journal of Rock Mechanics and Geotechnical Engineering*, vol. 14, no. 3, pp. 825–836, 2022.

[29] Q. Yin, J. Wu, Z. Jiang et al., "Investigating the effect of water quenching cycles on mechanical behaviors for granites after conventional triaxial compression," *Geomechanics and Geophysics for Geo-Energy and Geo-Resources*, vol. 8, no. 2, p. 77, 2022.

[30] Z. Dou, S. X. Tang, X. Y. Zhang et al., "Influence of shear displacement on fluid flow and solute transport in a 3D rough fracture," *Lithosphere*, vol. 2021, no. Special 4, p. 1569736, 2021.

[31] G. Han, Y. Zhou, R. Liu, Q. Tang, X. Wang, and L. Song, "Influence of surface roughness on shear behaviors of rock joints under constant normal load and stiffness boundary conditions," *Natural Hazards*, vol. 112, no. 1, pp. 367–385, 2022.

[32] Z. Wang, W. Li, and J. Chen, "Application of various nonlinear models to predict the uniaxial compressive strength of weakly cemented Jurassic rocks," *Natural Resources Research*, vol. 31, no. 1, pp. 371–384, 2022.

[33] H. Liu, D. Zhang, H. Zhao, M. Chi, and W. Yu, "Behavior of weakly cemented rock with different moisture contents under various tri-axial loading states," *Energies*, vol. 12, no. 8, p. 1563, 2019.

[34] B. Liu, Y. Zhao, C. Zhang, J. Zhou, Y. Li, and Z. Sun, "Characteristic strength and acoustic emission properties of weakly cemented sandstone at different depths under uniaxial compression," *International Journal of Coal Science & Technology*, vol. 8, no. 6, pp. 1288–1301, 2021.

[35] Y. Zhao and B. Liu, "Deformation field and acoustic emission characteristics of weakly cemented rock under Brazilian splitting test," *Natural Resources Research*, vol. 30, no. 2, pp. 1925–1939, 2021.

[36] H. Wang, T. Yang, and Y. Zuo, "Experimental study on acoustic emission of weakly cemented sandstone considering bedding angle," *Shock and Vibration*, vol. 2018, 12 pages, 2018.

[37] K. Develi and T. Babadagli, "Experimental and visual analysis of single-phase flow through rough fracture replicas," *International Journal of Rock Mechanics and Mining Sciences*, vol. 73, pp. 139–155, 2015.

[38] G. Fan, S. Zhang, B. Cao, D. Zhang, and C. Zhang, "Impact of mine panel size on hydraulic permeability of weakly cemented strata," *Sustainability*, vol. 12, no. 6, p. 2396, 2020.

[39] S. Zhang, G. Fan, D. Zhang et al., "Impacts of longwall mining speeds on permeability of weakly cemented strata and subsurface watertable: a case study," *Geomatics, Natural Hazards and Risk*, vol. 12, no. 1, pp. 3063–3088, 2021.

[40] L. Zou, L. Jing, and V. Cvetkovic, "Roughness decomposition and nonlinear fluid flow in a single rock fracture," *International Journal of Rock Mechanics and Mining Sciences*, vol. 75, pp. 102–118, 2015.

[41] S. Zhan, T. Wang, and T. Huang, "Variations of hydraulic conductivity of fracture sets and fractured rock mass with test scale: case study at Heshe well site in Central Taiwan," *Engineering Geology*, vol. 206, pp. 94–106, 2016.

[42] W. Zhong, J. Ouyang, D. Yang, X. Wang, Z. Guo, and K. Hu, "Effect of the in situ leaching solution of ion-absorbed rare earth on the mechanical behavior of basement rock," *Journal of Rock Mechanics and Geotechnical Engineering*, 2021.

[43] Y. Guo, X. Jiang, and Z. Song, "Analysis of seepage evolution law of rock mass based on the numerical algorithm considering strength weakening water absorption," *Arabian Journal of Geosciences*, vol. 11, no. 13, 2018.

[44] G. Fan, M. Chen, D. Zhang et al., "Experimental study on the permeability of weakly cemented rock under different stress states in triaxial compression tests," *Geofluids*, vol. 2018, 9 pages, 2018.

[45] Z. Liu, Z. Fan, and Y. Zhang, "Fracture characteristics of overlying bedrock and clay aquiclude subjected to shallow coal seam mining," *Mine Water and the Environment*, vol. 38, no. 1, pp. 136–147, 2019.

[46] R. S. Tandon and V. Gupta, "The control of mineral constituents and textural characteristics on the petrophysical & mechanical (PM) properties of different rocks of the Himalaya," *Engineering Geology*, vol. 153, pp. 125–143, 2013.

[47] H. Atapour and A. Mortazavi, "The influence of mean grain size on unconfined compressive strength of weakly consolidated reservoir sandstones," *Journal of Petroleum Science and Engineering*, vol. 171, pp. 63–70, 2018.

[48] V. Gupta and R. Sharma, "Relationship between textural, petrophysical and mechanical properties of quartzites: a case study from northwestern Himalaya," *Engineering Geology*, vol. 135, pp. 1–9, 2012.

[49] Z. Wang, W. Li, Q. Wang, S. Liu, Y. Hu, and K. Fan, "Relationships between the petrographic, physical and mechanical characteristics of sedimentary rocks in Jurassic weakly cemented strata," *Environmental Earth Sciences*, vol. 78, no. 5, 2019.

[50] S. Zhang, G. Fan, D. Zhang, M. Chen, and C. Zhang, "Study on material properties and similar material proportion of weakly cemented water-resisting strata," *Arabian Journal of Geosciences*, vol. 12, no. 11, 2019.

[51] Q. Meng, J. Wang, L. Han, W. Sun, W. Qiao, and G. Wang, "Physical and mechanical properties and constitutive model of very weakly cemented rock," *Rock and Soil Mechanics*, vol. 41, pp. 19–29, 2020.

[52] H. Li, K. Wang, H. Li, and C. Liu, "Study on mechanical and acoustic emission characteristics of weakly cementation sandstone in Shendong coal field," *Journal of Mining & Safety Engineering*, vol. 35, pp. 843–851, 2018.